

Influence of Spacer Frames for Wooden Roof Windows on the Formation of Surface Condensation

Martin Múčka,* Přemysl Šedivka, Jan Bomba, and Jaroslav Blažek

This study reports the thermal characteristics of windows installed in the roof cladding of a block of flats in the second temperature zone of the Czech Republic, with boundary conditions for the design value $\theta_{se} = -15$ °C, according to the national standard ČSN 73 0540-3 (2005). The thermal behaviour of these elements was evaluated with regard to the condensation on roof windows, with four different types of spacer frames and the given boundary conditions, for maintenance of the thermal and technical humidity comfort of the interior. The tests of the surface temperatures of the diagnosed glazed roof units at the glazing of the wooden windows demonstrated that the SGG composite spacer was the best from a thermal perspective. The spacer frames based on aluminum, stainless steel, and a combination of stainless steel and plastic (TGI) did not provide adequate thermal insulation characteristics for usage in roof windows under the given climatic conditions, and condensation occurred on the glass surfaces.

Keywords: Wooden roof window; Edge conditions; Spacer frames; Surface condensation; Air humidity; Thermal properties

*Contact information: Czech University of Life Sciences, Faculty of Forestry and Wood Sciences, Kamýčká 1176, 165 21 Prague 6 - Suchbátka, Czech Republic; *Corresponding author: mucka@fld.czu.cz*

INTRODUCTION

The heat transfer envelope of a building refers to not only opaque building structures but also to translucent structures (building aperture fillings), namely, the whole area of the building envelope that lies on the system boundary of the building and separates two environments with different thermo-humidity parameters. Compared with opaque structures, translucent structures are the most problematic parts from a solar, energy, and thermal viewpoint (Gustavsen *et al.* 2007).

In attic apartment units there is a deterioration of the thermal properties of translucent structures (insulating double glass) by about 20 to 30% (Fig. 1) (Popiel and Sobczak 2014) due to convective heat transfer in the air gap, usually because of the location of the sunroof with an angle less than 90° (angle of the window plane to the horizontal plane of the floor). However, in the case of roof windows, there is a concurrent increase in the efficiency of the energy balance of the concerned windows and the entire object, due to the direct brightness of the sky, by up to 40% as compared with a window positioned vertically (the plane of the window makes an angle of 90° with the plane of the floor) (Puškár *et al.* 2003). The climatic conditions in the Czech Republic according to temperature zones I through IV range from -16 °C to +35 °C (ČSN 73 0540-3 (2005)). In extreme conditions in alpine areas, the temperature drops to -25 °C or lower. In summer, the temperature in direct sunlight can be +45 °C or higher in exceptional cases. These are the known temperature differences in various temperature zones on a yearly basis, but it is

also necessary to consider the temperature fluctuations between day and night (Tywoniak 2005).

The consequence of the above (high temperature gradient) along with an inadequate exchange of air in the interior (higher humidity in the object) may result in a drop in the surface temperature of the structure (glass panel) below the dew point θ_{dp} , which for $\theta_i = 20$ °C and $\varphi_i = 50\%$ is approximately 9.3 °C (48.74 °F), and gradual condensation of the air humidity and subsequent formation of mildew on the inner side of the glass (position 4) and window profiles. This state may transition to progressive and irreversible destruction of the surface of the wooden window frames. At the same time, spores are released into the air and create conditions for the occurrence of chronic respiratory diseases, allergies, and asthma (Wei *et al.* 2010; Zhong *et al.* 2014).

One possible method for preventing negative abiotic and biotic factors is the use of a suitable window profile of the casement and frame in combination with a suitable type of energy glass, as well as the use of a suitable spacer (Stirling *et al.* 2002). Further methods include the application of new types of low-emission surface finish coatings for the window structures that reduce material emissivity (Reinprecht and Pánek 2015). Another way to improve the thermal properties of the windows is to use suitable sealing for the structural and functional joints of the windows and circumferential fittings, warm edges between the glass panels, and other suitable building construction indicators (Bergh *et al.* 2013).

The aim of this paper was estimation of the degree of formation of condensation between the glass and window frame (in the glazing joint) in varying climatic conditions. Also the elimination of the condensation between the glass panels through the use of new types of standard types and warm edge spacers was studied. This article provides guidance in choosing the most appropriate spacer for use between panes under particular weather conditions.

EXPERIMENTAL

Methods

The study determined the surface temperature on double glazing by direct experimental measurement using temperature sensors in risk areas to diagnose the dew point temperature (θ_{dp}) and local heat transmittance coefficient (U_g). For each experimental measurement, standard insulating double glass was used with $U_g = 1.1$ W m⁻² K⁻¹, with a wooden frame having a bonded profile from three lamellae. The lamellae were made of spruce wood. The structural design is shown in Fig. 2. The protective coating was a water-based glaze applied using high-pressure technology.

The test windows were installed facing north on the 4th floor in the attic rooms of a block of flats, at a height of 227 m above sea level in the town of Kuřim, Czech Republic. According to ČSN 73 0540-3 (2005), this is in temperature zone 2, where the average temperature of the exterior air in winter (θ_e) is 5.1 °C. The windows were mounted in the roof structure at an angle of 35° (Figs. 3 and 4). Measurements were taken at 30-min intervals throughout the day and night (from 07:00 to 06:30 on the following day). Each measured value was repeated 6 times consecutively to limit measurement errors. For all roof windows, the measurement applied to variables that change with the edge conditions of the given temperature locality, and the diagnosis of the concerned structures applied to the thermal properties of the spacers of the insulating double glass.

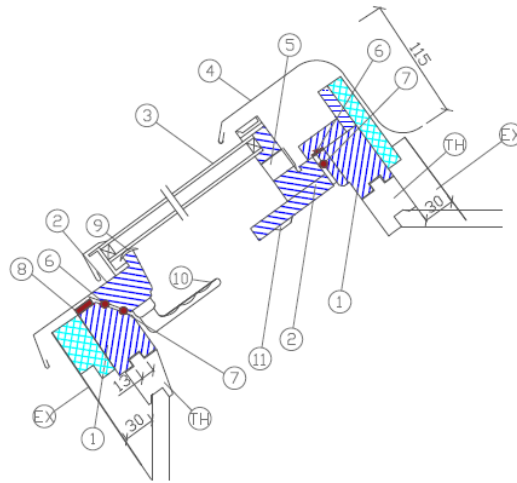


Fig. 1. Design of the test window. (1) window frame; (2) casement; (3) window glass; (4) window flashing; (5) ventilation opening; (6) I. grade seals; (7) II. grade seals; (8) III. grade seals; (9) condensate drain; (10) window handle; (11) switching mechanism; TH, thermstrips; EX, extruded polystyrene

For all roof windows, the measurement applied to the relative air humidity in the interior (φ_i), interior air temperature (θ_i), external air temperature (θ_e), dew point temperature (θ_{dp}), and surface temperature of the insulating glass around the perimeter of the glazing in the interior (θ_{si}). The thermal properties of the spacers were determined under the given edge conditions. The characteristic value that determines the possibility for formation of condensate on the interior surface of the insulating glass is the dew point value, which is determined by comparison of the (measured) relative air humidity on the surface (φ_{si}) and the maximum relative air humidity ($\varphi_{i \max}$) at which condensation forms on the insulating glass in the interior.

The thermal properties of structures (translucent and opaque) is precisely detected on the basis of empirical calculations in two ways: (i) the heat factor (ČSN 73 0540 (2005)), which was not considered because it is inconclusive and inaccurate; and (ii) the ascertained saturation of water vapour in the air and partial water vapour pressures in the air. On the basis of empirical surveys, it is possible to calculate the maximum relative moisture content ($\varphi_{i \max}$) at which the air is fully saturated with water vapour at a given temperature (θ_{si}), and thus when this limit is exceeded, condensation is formed.

The empirical calculation for the saturation pressure of water vapour at $\theta < ^\circ\text{C}$ and at $\theta \geq ^\circ\text{C}$ are shown in Eqs. 1 and 2, respectively. Equation 3 shows the calculation of the maximum relative air humidity at which condensation is not formed on the insulating glass in the interior,

$$p_{sat} = 610,5 \cdot e^{\frac{21,875 \cdot \theta}{265,5 + \theta}} \quad (1)$$

$$p_{sat} = 610,5 \cdot e^{\frac{17,269 \cdot \theta}{237,3 + \theta}} \quad (2)$$

$$\varphi_{i \max} = \frac{p_{sat}(\theta_{si})}{p_{sat}} \cdot 100 \quad (3)$$

where e is the Euler number (base of natural logarithms; $e = 2.718$), $p_{\text{sat}}(\theta_{\text{si}})$ is the partial saturation pressure upon change of measured surface temperature θ_{si} on the glass in the interior (Pa), p_{sat} is the partial pressure of saturated water vapours at an air temperature of θ_i in the interior (Pa), and $\varphi_{i \text{ max}}$ is the maximum relative air humidity at which condensation is not formed on the insulating glass in the interior (%).

The empirical calculation of surface relative air humidity is shown in Eq. 4,

$$\varphi_{\text{si}} = \frac{p_{\text{di}}}{p_{\text{sat}}(\theta_{\text{si}})} \cdot \varphi_i \quad (4)$$

where p_{di} is the partial pressure of water vapour in the air in the interior at the given temperature θ_i (Pa), $p_{\text{sat}}(\theta_{\text{si}})$ is the partial saturation pressure at a measured surface air temperature of θ_{si} on the glass in the interior (Pa), and φ_{si} is the surface relative air humidity (measured) (%).

The first risk area, in the sense of low surface temperature on the inner side of the insulating double glass, for formation of water vapour condensation is the point of connection of the glazing unit to the frame of the window casement around the perimeter of the glazing, *i.e.*, in the so-called glazing half groove (glazing joint). The second risk area is the cold edges of the glazing unit (Elek and Kovács 2014). Values were set by mutual comparison of the values $\varphi_{i \text{ max}}$ and φ_{si} (Figs. 6 to 10). The results were evaluated at a significance level of $\alpha = 95\%$ using the regressive analysis (STATISTICA, version 12, StatSoft CR s.r.o., Prague, Czech Republic).

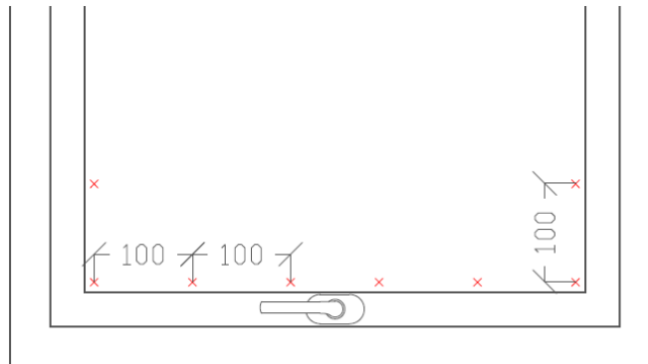


Fig. 2. Diagram of the positioning of the temperature sensors on the inside of the insulating double glazing in the lower area of the glazing

To determine the surface temperatures on the insulating double glass at the corners of the window structure, the so-called "guarded hot box" measuring method was applied. The distribution of the sensors is shown in Figs. 3 and 4. To determine the surface temperature of the insulating glass, the contact probe method was used with contact probes type 0614.1635/301 (Testo AG, Mönchaltorf, Germany), where the contact sensors were connected to the surface on the inner side of the insulating double glazing and the surface temperature data (θ_{si}) were averaged and transferred to device T635-2 type 0560.6352 with serial number 02502099 (Testo AG, Mönchaltorf, Germany). The temperature and humidity sensors in the interior also measures the dew point temperature (θ_{dp}), where the dew point temperature is a function of the temperature and relative humidity ($\theta_{\text{dp}} = f(\theta_i, \varphi_i)$).



Fig. 3. Positioning of the temperature sensors on the inside of the insulating double glazing in the lower area of the glazing

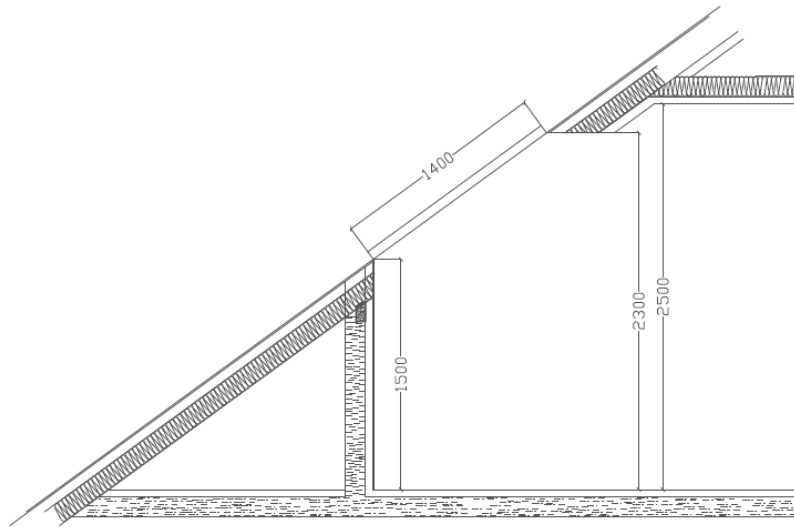


Fig. 4. Test windows and experimental device

The temperature (θ_e) and humidity (φ_e) on the exterior was determined using a radio probe type DR FID 199/05540189 (Testo AG, Mönchaltorf, Germany). The surface temperature of the structure when using the coefficient α_i was used to calculate the local heat transmittance coefficient U value ($\text{W m}^{-2} \text{K}^{-1}$). This physical variable determines how much heat energy is transmitted through a given surface at a given temperature gradient over a given time period.

Table 1. Overview of Measured Commercial Spacer Systems and their Available Dimensions and Properties


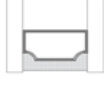
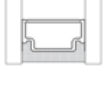

Spacer Type	Product description and material properties	Illustration	λ_{eq} (W m ⁻² K ⁻¹)	Spacer bar width w, (mm)	Dimensions and parameters applied in calculating conductivity: thickness (t), primary sealant, width (w), secondary sealant	Further information
Aluminium	Hollow aluminium spacer profile		4.89 - 6.50	6.5	t = 16 mm, w = 9 mm	HZB spol. s.r.o. http://www.okna-roto.cz/
Stainless Steel	Wall thickness 18 mm		0.78 - 0.82	6.5	t = 16 mm, w = 8 mm	Attl a spol. s.r.o. http://www.attl.cz/
TGI	Stainless Steel [thickness 0.10 mm, $\lambda = 15$ W m ⁻² K ⁻¹] with plastic top [thickness 0.6 mm, $\lambda = 0.195$ W m ⁻² K ⁻¹]		0.34 - 0.34	7.0	t = 16 mm, w = 8 mm	Rover s.r.o. http://www.rover-lbc.cz/
SGG [Swisspacer]	Composite plastic S AN [styrol acryl nitril copolymer with 35% glass fiber, thickness 1.0 mm, $\lambda = 0.16$ W m ⁻² K ⁻¹] with thin aluminium membrane [thickness 0.003 mm, $\lambda = 160$ W m ⁻² K ⁻¹]		0.56 - 0.62	6.5	t = 16 mm, w = 9 mm	DAKO spol. s.r.o. http://www.nizkoe-nergeticky.cz/

Table 1 shows the four types of frames (aluminium, stainless steel, TGI, and SGG) that were measured in the given project. Their physical characteristics were determined, and the influence of the spacers used on the thermal characteristics of the measured translucent roof structures was compared.

RESULTS AND DISCUSSION

Figure 5 shows the curves of the individual surface temperatures of the spacers used with a different material base and different thermal characteristics. The measured surface temperatures recorded over a period of 24 h under real-time edge temperature conditions, were $\theta_e = -1.92$ °C to $+2.71$ °C on the exterior and $\theta_i = 18.91$ °C to 23.38 °C in the interior.

Table 2. Relative Air Humidity and Temperature on the Interior Glass Surface

	φ_{si} [Aluminium]		φ_{si} [Stainless Steel]		φ_{si} [TGI]		φ_{si} [SGG]	
	φ_{si} relative air humidity (%)	θ_{si} air temperature (°C)	φ_{si} relative air humidity (%)	θ_{si} air temperature (°C)	φ_{si} relative air humidity (%)	θ_{si} air temperature (°C)	φ_{si} relative air humidity (%)	θ_{si} air temperature (°C)
X (%)	97.17	10.38	87.67	11.98	68.56	15.17	64.21	16.61
Max. (%)	99.93	11.51	95.39	12.96	69.84	16.22	65.40	17.92
Min. (%)	94.12	9.23	84.09	10.71	67.10	14.21	63.10	15.11
SD	1.69	0.59	1.98	0.59	1.96	0.47	1.21	0.51
v (%)	1.74	5.57	2.26	4.91	1.73	3.11	0.98	3.59

X, average value; Max., maximum measured value; Min., minimum measured value; SD, standard deviation; v, coefficient of variation

The results were evaluated at a significance level of $\alpha = 95\%$ using an analysis of variance (ANOVA), and the difference of individual groups was determined using a post-hoc test (Tukey HSD test). The results of the analysis of variance are shown in Figs. 6 to 10. The measured values are specified in Table 2.

The graphical dependency of the aluminum spacer was on the edge limit of the dew point temperature for the given interior temperature and relative humidity. The best values (high surface temperature) were characteristic of the insulating double glass with SGG spacers, followed by the TGI, stainless steel, and aluminum spacers. From a statistical viewpoint, the aluminum and stainless steel spacers had a higher standard deviation θ_{si} than the TGI and SGG spacers. This result confirmed that the aluminum and stainless steel spacers had higher heat conductivity and worse insulating characteristics.

The results in terms of the values of surface temperatures θ_{si} , involving the dew point, corresponded to comparing actual average values of surface relative humidity φ_{si} over time at the spacers used in types of insulation double glazing (Figs. 7 and 8).

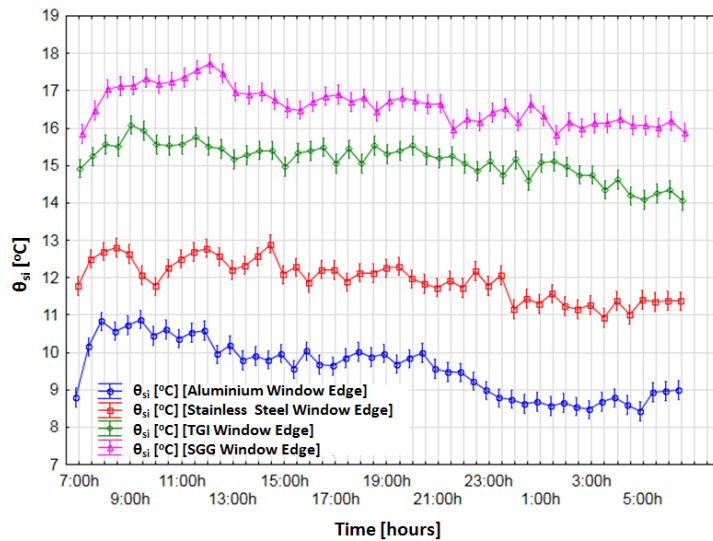


Fig. 5. Average measured surface temperatures θ_{si} on the insulating double glass over time for the four types of window spacer frames

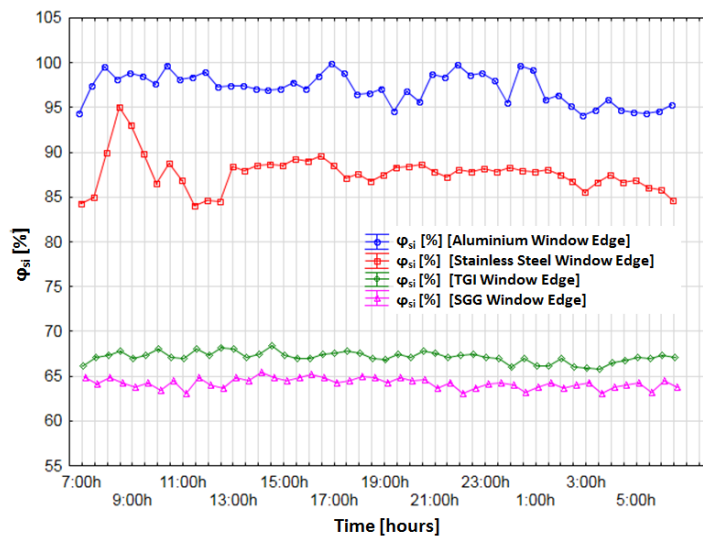


Fig. 6. Average measured surface relative air humidity φ_{si} over time for different window spacer frames

Figures 6 to 10 characterise the curve of the relative air humidity (φ_{si} , $\varphi_{i\ max}$) over time. In the case of the aluminum and stainless steel spacers, condensation of air humidity occurred on the inner cooled insulating glass under the given boundary conditions (Figs. 7 and 8).

For the tested type TGI spacer (Fig. 9), condensation of air humidity occurred on the insulating glass on the interior, but the difference between the relative air humidity φ_{si} and maximum relative air humidity $\varphi_{i\ max}$ was much lower than in the case of spacers of the aluminum (Fig. 7) and stainless steel (Fig. 8) types under the defined boundary conditions.

In all graphs, the surface relative air humidity (shown in red) exceeded the maximum relative humidity (shown in blue), which is depicted by the concerned condensation field.

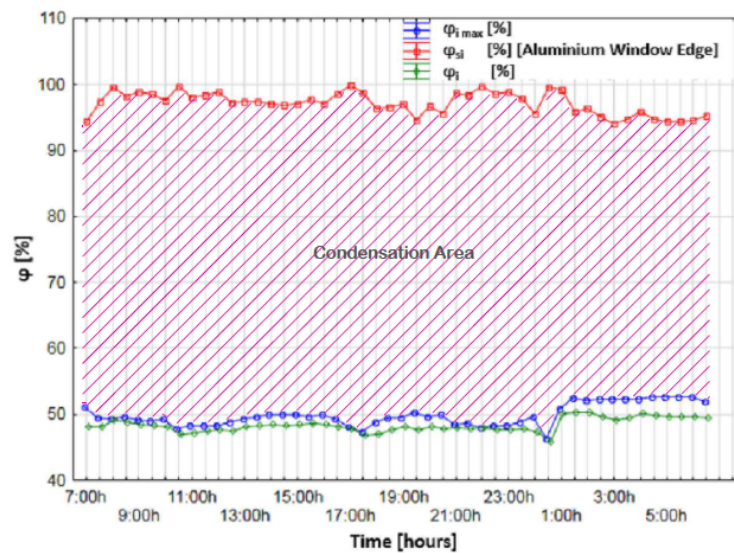


Fig. 7. Average measured humidity values φ_i , φ_{si} , and $\varphi_{i\ max}$ over time for the aluminum spacer frame

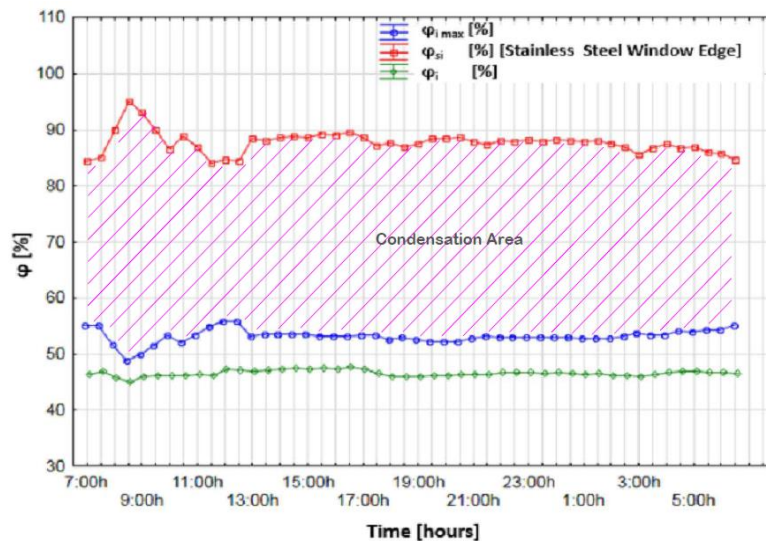


Fig. 8. Average measured humidity values φ_i , φ_{si} , and $\varphi_{i\ max}$ over time for the stainless steel spacer

By their parameters, the window spacers fulfill the requirements for thermal insulating characteristics under the defined boundary conditions of the Swisspacer SGG type of spacer, which was the only spacer for which the surface relative humidity (shown in red) did not exceed the maximum relative humidity (shown in blue). The relative air humidity values φ_{si} did not exceed the maximum relative air humidity values $\varphi_{i \max}$ over the entire measurement period under the given boundary conditions (Fig. 11). Thus, when using the insulating Swisspacer SGG spacer there was no condensation on the inner side of the insulating double glazing, and the conditions for the thermal insulating characteristics of the window structure were fulfilled.

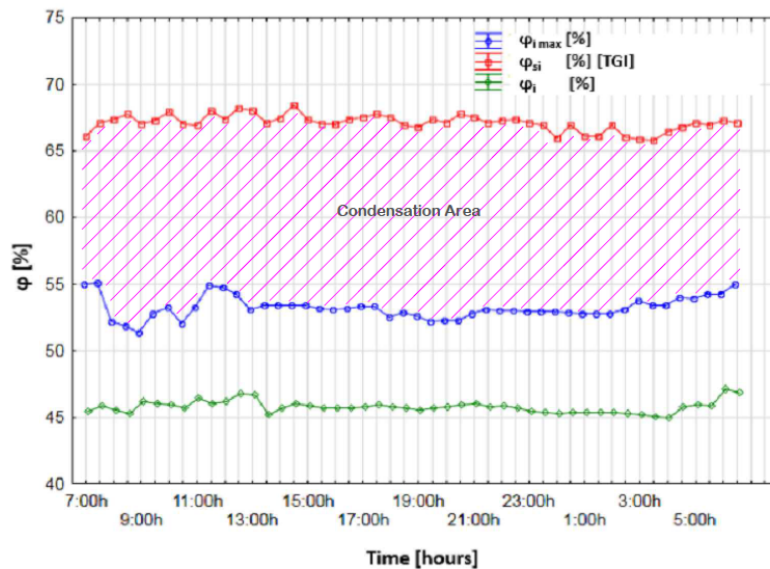


Fig. 9. Average actual measured humidity values φ_i , φ_{si} , and $\varphi_{i \max}$ over time for the TGI spacer

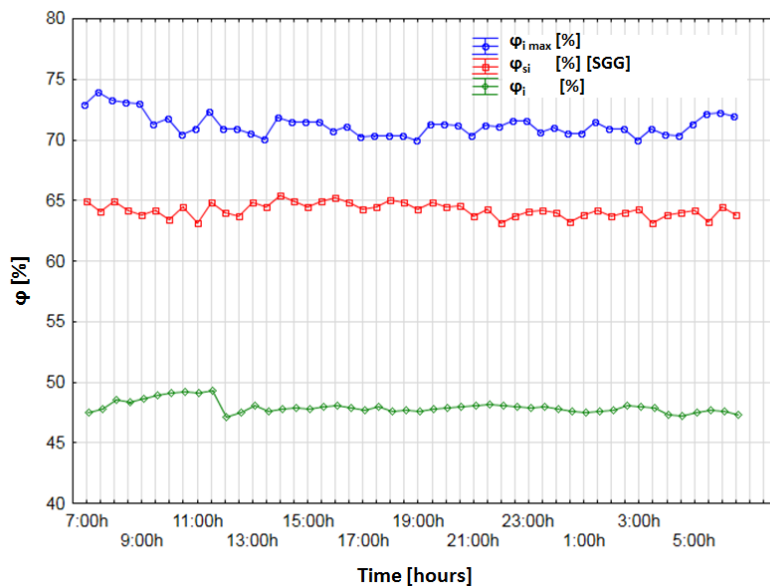


Fig. 10. Average actual measured humidity values φ_i , φ_{si} , and $\varphi_{i \max}$ over time for the SGG spacer

CONCLUSIONS

1. Measurement of the surface temperatures of the diagnosed glazed roof units at the glazing of the wooden windows (highest linear heat transmittance coefficient) showed that the SGG composite spacer was best from a thermal perspective, having a high surface temperature within the given boundary temperature and humidity conditions. It is important to never exceed the maximum of surface relative humidity (φ_{si}) at a given partial pressure at which water vapour condensation occurred on the roof windows.
2. The aluminum, stainless steel, and TGI spacers had varying heat conductance, which deteriorated the linear heat transmittance coefficient.
3. Scientific publications recommend warm spacers, including TGI spacers. The results presented here demonstrated that with a minimum change in temperature and humidity boundary conditions using TGI spacers in the wooden frames of roof windows, there is a drop in the surface temperature and a rise in the interior surface humidity above the humidity level for which the maximum water vapour saturation of the air is reached ($p_{sat} = 100\%$). The structure did not show adequate thermal insulation characteristics, and condensation occurred.

ACKNOWLEDGMENTS

This work has been funded by the research project “Measurement of heat transfer coefficient”, No. A09/15, from the Czech University of Life Sciences Prague.

REFERENCES CITED

- Bergh, S. V. D., Hart, R., Jelle, B. P., and Gustavsen, A. (2013). “Window spacers and edge seals in insulating glass units: A state-of-the-art review and future perspectives,” *Energy and Buildings* 58, 263-280. DOI: 10.1016/j.enbuild.2012.10.006
- ČSN EN 14 351 (2011). “Windows and doors – Product standard, performance characteristics – Part 1: Windows and external pedestrian door sets without resistance to fire and/or smoke leakage characteristics,” Office for Standards, Metrology and Testing, Prague, Czech Republic.
- ČSN 73 0540-3 (2005). “Thermal protection of buildings – Part 3: Design value quantities,” Czech Standards Institute, Prague, Czech Republic.
- ČSN 74 6101 (2015). “Timber windows – Basic regulations,” Office for Standards, Metrology and Testing, Prague, Czech Republic.
- Elek, L., and Kovács, Z. (2014). “Impact of the glazing system on the U-Factor and inside surface temperature of windows,” *Acta Polytechnica Hungarica* 11(8), 197-213.
- Gustavsen, A., Jelle, B. P., Arasteh, D., and Kohler, C. (2007). *State-of-the-Art High Insulating Window Frames – Research and Market Review* (Project Report 6), SINTEF Building and Infrastructure, Oslo, Norway.
- Popiel, C. O., and Sobczak, M. (2014). “Effect of roller blinds on heat losses through a double-glazing window during the heating season in Central Europe,” *Energy and Buildings* 74, 48-58. DOI: 10.1016/j.enbuild.2014.11.047

- Pušár, A., Fučila, J., Szomolányiová, K., and Mrlík, J. (2003). *Windows, Doors, Glass Walls*, Jaga Group v.o.s., Bratislava, Slovakia, 28-36.
- Reinprecht, L., and Pánek, M. (2015). “Effects of wood roughness, light pigments and water repellent on the color stability of painted spruce subjected to natural and accelerated weathering,” *BioResources* 10(4), 7203-7219. DOI: 10.15376/biores.10.4.7203-7219
- Stirling, Ch., Road, K., and Kilbride, E. (2002). *Thermal Insulation: Avoiding Risk*, BRE Press London, United Kingdom, 1-85
- Tywniak, J. (2005). *Low-Energy Houses: Principles and Examples*, Grada Publishing, Prague, Czech Republic.
- Wei, J., Zhao, J., and Chen, Q. (2010). “Energy performance of a dual airflow window under different climates,” *Energy and Buildings* 42, 111-122. DOI: 10.1016/j.enbuild.2009.07.018
- Zhong, S. Li, K., Zhou, Y., and Zhang, X. (2014). “Comparative study on the dynamic heat transfer characteristics of a PCM-filled glass window and hollow glass window,” *Energy and Buildings* 85, 483. DOI: 10.1016/j.enbuild.2014.09.054

Article submitted: March 2, 2016; Peer review completed: May 1, 2016; Revised version received: May 18, 2016; Accepted: May 20, 2016; Published: May 31, 2016.
DOI: 10.15376/biores.11.3.6174-6184